06,13

Dielectric characteristics of heteroepitaxial $Sr_{0.60}Ba_{0.40}Nb_2O_6$ thin films grown on a Pt(001)/MgO(001) substrate

© N.V. Makinyan[1,2], A.V. Pavlenko[1,2]

[1] Southern Scientific Center, Russian Academy of Sciences, Rostov-on-Don, Russia
[2] Scientific Research Institute of Physics, Southern Federal University, Rostov-on-Don, Russia

E-mail: norair.makinyan@yandex.ru

Received August 30, 2023
Revised September 27, 2023
Accepted September 28, 2023

The structure, surface microstructure, dielectric and ferroelectric characteristics of thin films of barium-strontium niobate $Sr_{0.60}Ba_{0.40}Nb_2O_6$ (SBN60) grown on a Pt(001)/MgO(001) substrate have been studied. It is shown that the films are unalloyed, monocrystalline, and by the nature of changes in the dielectric permittivity (ε' and ε'') from the temperature and frequency of the measuring electric field, they are relaxor ferroelectrics. It is established that in the investigated film the Burns temperature is 475 K, the Vogel–Fulcher temperature is 367 K, and in the vicinity of $T = 150$ K there is a phase transition between two ferroelectric phases. It is shown that at room temperature, depending on the electric field strength, the prevailing charge transport mechanisms in SBN60 films are Poole–Frenkel emission and space charge limited current. The reasons for the revealed patterns are discussed.

Keywords: dielectric characteristics, relaxor ferroelectric, tetragonal tungsten bronze, leakage currents.

DOI: 10.61011/PSS.2023.11.57321.192

1. Introduction

Ferroelectric (FE) materials in the form of nanoscale films have been attracting attention in the physical materials science for a long time, which is associated with the prospects for their use in microelectronics and nanoelectronics [1]. Well-studied are multicomponent complex oxides with a structure of perovskite type ($PbZr_{1-x}Ti_xO_3$, $Ba_{1-x}Sr_xTiO_3$, $NaNbO_3$) and tetragonal tungsten bronze (TTB) type ($Sr_{1-x}Ba_xNb_2O_6$ (SBN), $Ba_2NaNb_5O_{15}$), and single crystals of $SrTiO_3$, MgO, Al_2O_3, and Si of various orientations are used mainly as substrates for film growth. The phase composition, structure, microstructure, and physical properties of thin films depend significantly both on the method of their synthesis and on the features of the manifestation of size effects [2]. Deformation of the lattice cell of such materials can result in a significant change, for example, in the values of the relative dielectric constant, the values of spontaneous polarization and temperatures of phase transformations, as well as the implementation of phases not observed in powders, ceramics, and single crystals [3]. This opens up new ways to produce materials with the required parameters and generates interest in this area.

Barium-strontium niobates are representatives of FEs with the TTB structure. Large values of relative dielectric constant (up to 25000), piezoelectric constant (up to 650 pC/N), and pyroelectric constant ($0.065\,\mu C \cdot cm^{-2} \cdot K^{-1}$) make them promising in the development of optical modulators, uncooled pyroelectric detectors, and piezoelectric sensors [4–6]. Despite a significant number of studies devoted to establishing the patterns of formation of dielectric and ferroelectric characteristics of thin SBN films, contradictions often take place in the literature about the temperatures of phase transformations and optical properties. As for leakage currents that restrict the use of film materials [7–9], their current values are mainly analyzed depending on the conditions of their manufacture [10,11], and the mechanisms are almost not studied. In [12], we have shown that for the synthesis of thin SBN films, the method of RF cathode sputtering is quite effective, when the entire technological process is carried out in an oxygen atmosphere, and the composition of the films corresponds to the composition of the ceramic target used for sputtering [3,12]. Taking into account the above, it is relevant to establish the patterns of formation of dielectric characteristics, mechanisms of leakage currents, and temperatures of phase transformations in SBN60 heteroepitaxial films grown by this method, which became the goal of this study.

2. Methods of fabrication and investigation of samples

SBN60 films with a thickness of ~ 1000 nm (estimated by the deposition time) on a Pt(001)/MgO(001) substrate were grown by high-frequency cathode sputtering of a ceramic target with the stoichiometric composition of $Sr_{0.60}Ba_{0.40}Nb_2O_6$ (manufactured at the SFU Physics Research Institute) in an oxygen atmosphere. The working gas pressure was 67 Pa, the initial substrate temperature was 673 K, and the input RF power was 135 W.

To carry out dielectric measurements in the direction perpendicular to the surface, samples were prepared with a Pt(001) layer with a thickness of ~ 150 nm as the bottom electrode and an Ag/Pd layer as the top electrode deposited by magnetron sputtering in an argon atmosphere using an Emitech SC7620 set-up, through a mask with a hole diameter of $90-100\,\mu$m.

X-ray diffraction studies were carried out on a „RIKOR" multifunctional X-ray unit (goniometer with a step of up to 0.001° (Crystal Logic Inc.); BSV21-Cu X-ray tube („Svetlana-Roentgen" JSC), scintillation detector (ITC „Radikon" LLC). The surface morphology was studied using a „Ntegra Academia" atomic force microscope by NT-MDT (Russia) at a temperature of 295 K. Scanning was carried out in semi-contact mode using a NS15/50 silicon cantilever (equipment of the Joint Center for Scientific and Technological Equipment of the Southern Scientific Center of the Russian Academy of Sciences (research, development, testing) № 501994.

The real (ε') and imaginary (ε'') parts of the complex dielectric constant in a frequency range of $f = 500-10^5$ Hz and a temperature range of $T = 80-500$ K were measured by an automated measuring unit based on an Agilent 4980A LCR meter and a Linkam THMS600 stage cryosystem. Dynamic dielectric hysteresis loops ($P(E)$) were measured by a TFAnalyzer2000 and a MST4000A analytical probe station. For the positive and negative branches of $P(U)$ the residual polarization (P_r), coercive field (E_c), maximum polarization ($P_{\max}$) were calculated in the „Hysteresis Software" program. Leakage currents were measured using TFAnalyzer2000.

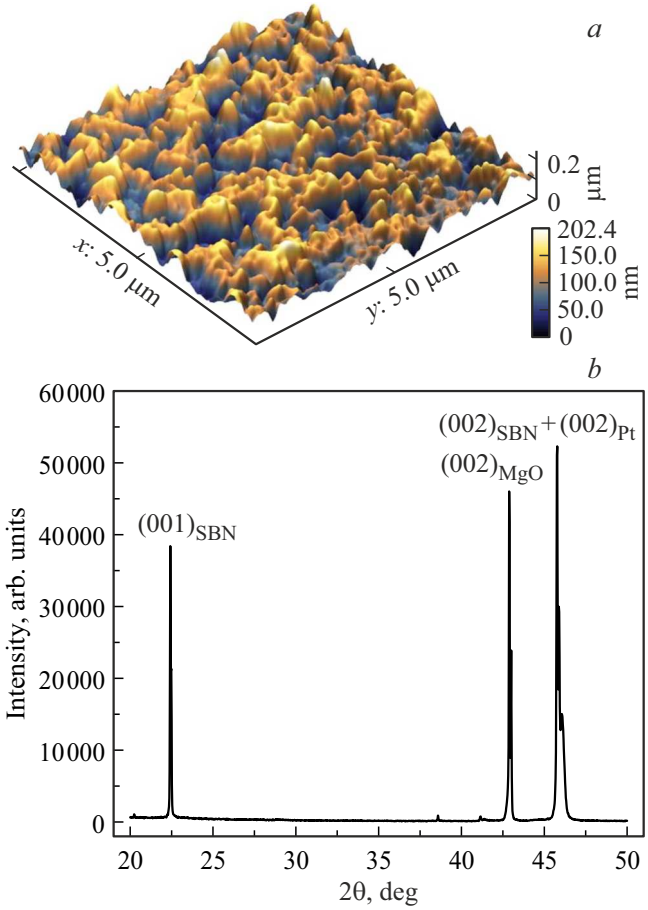

Figure 1. AFM image of the surface of the SBN60/Pt/MgO heterostructure in a typical area of $25\,\mu$m^2 (a); $\theta-2\theta$-X-ray diffraction pattern of the SBN60/Pt/MgO heterostructure (b).

3. Experimental results and discussion

According to the atomic force microscopy data (Figure 1), the surface of the SBN60 film is quite homogeneous, there were no cavities and other surface defects, and its root-mean-square roughness in a typical area of $5 \times 5\,\mu$m^2 was 33.25 nm. There were no signs of the presence of impurity inclusions on the surface of the film.

According to the X-ray diffraction analysis of the SBN60/Pt/MgO(001) heterostructure, it was established that both the Pt electrode and the SBN60 film were produced epitaxially on the MgO(001) substrate. In the $\theta-2\theta$ X-ray diffraction patterns in a scanning angle range of $20-50°$ only lines (00l) corresponding to the SBN60 and Pt layers and the MgO(001) substrate were recorded, which indicates the absence of impurity phases in the sample. The arrangement of maxima in the φ scanning of reflections (221) of the SBN60 film relative to the positions of maxima of reflections (113) of the MgO substrate indicated the formation of two types of orientation domains with their crystallographic axes rotated relative to the MgO axes by $\pm 18.4°$ as is the case with the direct deposition of SBN61 films of similar composition on MgO(001) [13]. The platinum film is formed with a completely parallel orientation of the crystallographic axes relative to the magnesium oxide.

The presence of ferroelectric properties in the SBN60 film at room temperature was proven by measuring dielectric hysteresis loops (Figure 2, a).

The $P(E)$ dependences had a loop-like shape typical for ferroelectrics, which in low fields was characterized by asymmetry, and with a further increase in E became almost symmetrical. As can be seen from Figure 2, b the values of $P_r, P_{\max}, E_c$ increased as the amplitude of the electric field increased and at $E = 80$ kV/cm they were $8.6\,\mu$ C/cm^2, $20.83\,\mu$C/cm^2, and 16.3 kV/cm, respectively. When an electric field with strength of $E > 80$ kV/cm was applied, electrical conductivity began to make a significant contribution to the measured response of SBN60 films (rounding of the loop ends occurred, breakdowns and degradation of the electrodes took place), which complicated the measurement process and the correct calculation of P_r, $P_{\max}$, E_c. For the same reason, we have failed to carry out correct measurements of the $P(E)$ dependences at $T > 398$ K. It can be seen from the $P_r(T)$ dependence of the SBN60 film shown in Figure 2, c that the phase

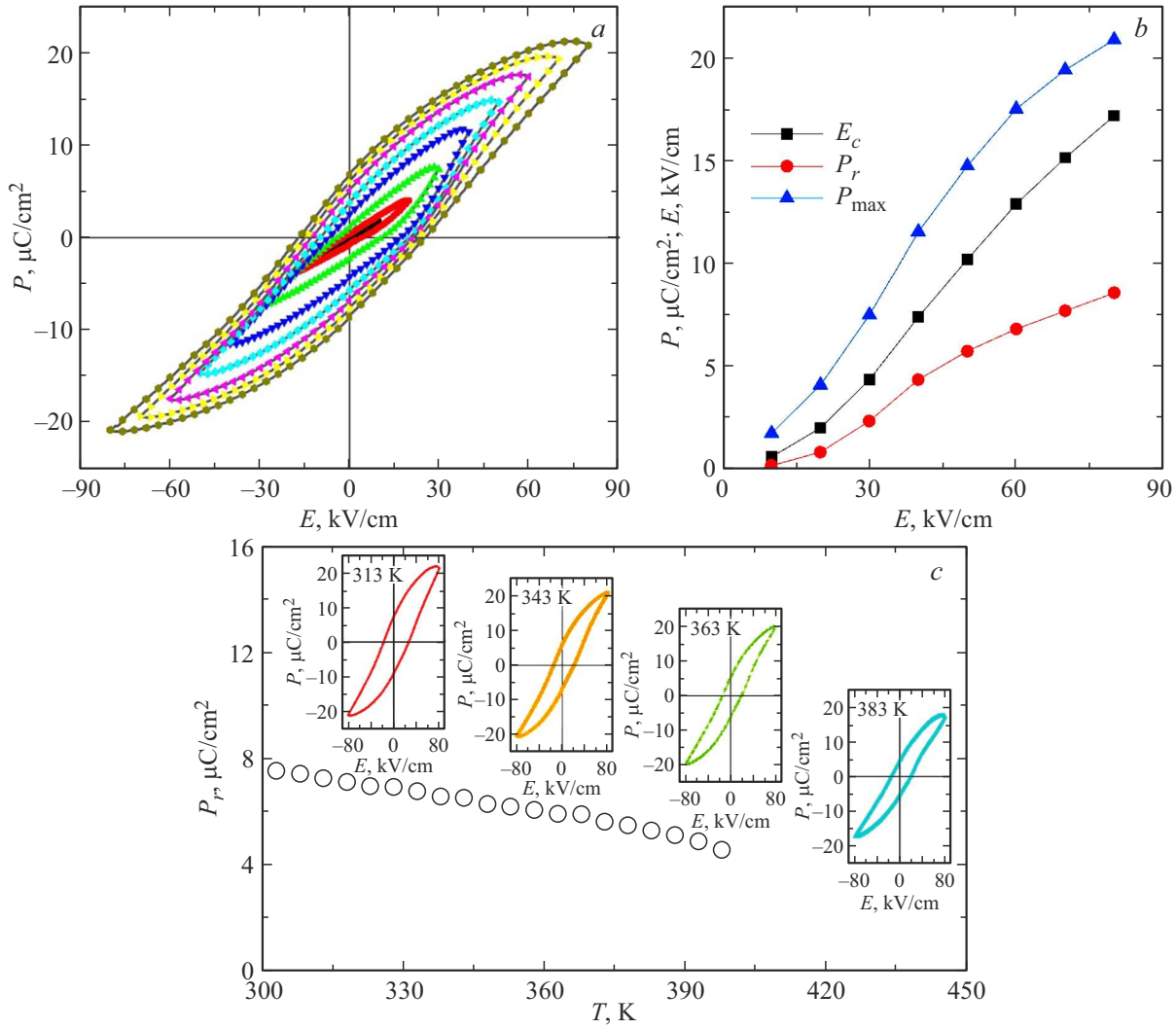

Figure 2. Dependence of $P(E)$ and P_r, $P_{\max}$, E_c on amplitude E at room temperature of the SBN60 film (a, b). Dependence of $P(E)$ and P_r in a temperature range of $T = 308-398$ (c).

transition to the paraelectric phase (PE) in the sample occurs at temperatures above 398 K.

To establish the mechanisms of leakage currents in the SBN60 film, current densities J as function of E were analyzed. The measurements were carried out with a „stair" voltage change. To exclude the component caused by polarization switching from the measured current, the films were pre-polarized with a voltage of the same polarity. The current was measured with a delay of $t_{\text{delay}} = 2\,\text{s}$ after the next voltage increment by $U = 0.1\,\text{V}$. In thin films, there are several main types of electrical conductivity, associated both with effects in the near-electrode region and with the bulk properties of the dielectric layer [14]. The first group includes mainly Schottky emission, and the second group includes Poole–Frenkel emission (PF) and space charge limited current (SCLC), each of which is characterized by its own law of change — $J(E)$ [14]. By plotting the obtained experimental dependences $J(E)$ in coordinates of $\ln(J)$ — $E^{1/2}$, $\ln(J/E)$ — $E^{1/2}$ and $\ln(J)$ — $\ln(E)$ and by carrying out the appropriate analysis, it is possible to establish which of the noted mechanisms prevails and in which fields. For SCLC, the slope coefficient should be close to two, because the dependence of the current density is directly proportional to the square of the field strength. For Schottky and PF emission, the slope coefficient of the straight line in the linear section is used to calculate the refraction index (n) of the material under study [15]. By comparing the refraction indices calculated from the experimentally obtained dependence $J(E)$ (using the expression I and the equation $n = \varepsilon_i^{1/2}$ [15]) and measured by optical methods, we can determine predominant conduction mechanism. The expression for dielectric constant has the following form:

$$\varepsilon_i = \frac{q^3}{\pi\varepsilon_0 b(Kk_{\text{B}}T)^2}, \qquad (1)$$

where q is electron charge, $1.6 \cdot 10^{-19}$ C; ε_0 is dielectric constant of vacuum, $8.85 \cdot 10^{-12}$ F/m; k_{B} is Boltzmann con-

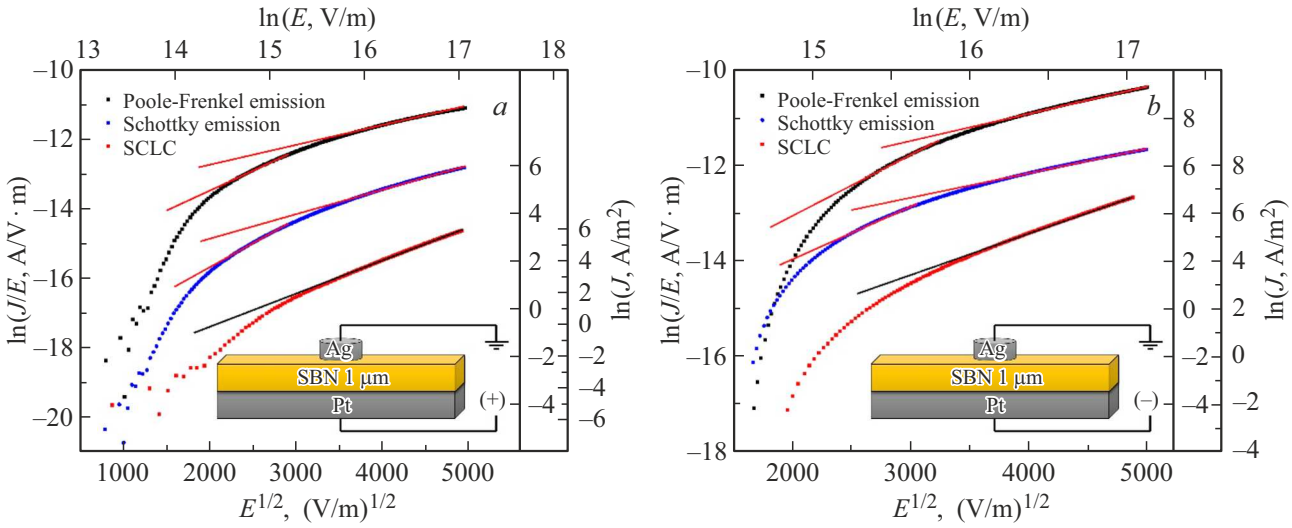

Figure 3. The leakage current density as a function of the electric field strength for positive (a) and negative (b) external fields in Poole–Frenkel coordinates ($\ln(J/E)-E^{1/2}$), Schottky coordinates ($\ln J-E^{1/2}$), SCLC ($\ln J-\ln E$) in the SBN60 film.

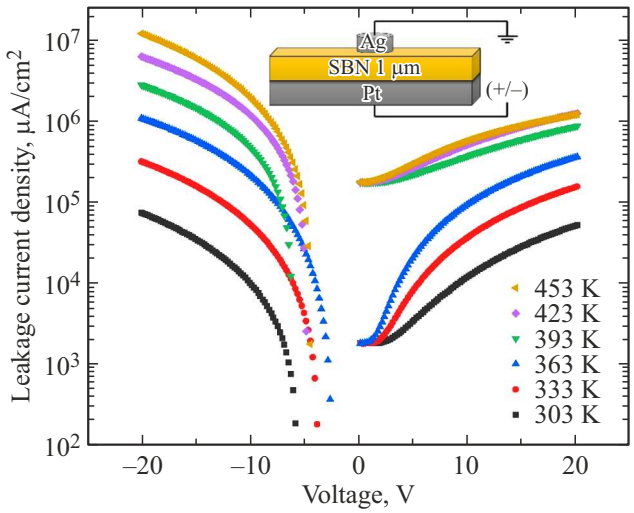

Figure 4. Temperature dependences of leakage current density in the SBN60 film.

stant, $1.38\cdot10^{-23}$ J/K; T is temperature, K; b is parameter equal to 4 and 1 in the case of Schottky and PF emission, respectively.

The $J(E)$ dependences for the SBN60 film plotted in the corresponding coordinates are shown in Figure 3, *a, b*.

In the SBN60 film, reliable results within the framework of the analyzed models are obtained only in the region of $E = 4.5-9.5$ MV/m, where the predominant conductivity mechanism is Poole–Frenkel emission. The above is also confirmed by the symmetry of the slope of the linear sections, regardless of the polarity of the external electric field (Figure 3, *a* and *b*). As E increases, it can be observed that the slope coefficient for the SCLC is increasingly approaching the value of 2, i. e. starting from $E = 10$ MV/m the conductivity is determined by the space charge limitation. When analyzing the temperature dependences (Figure 4), it was established that up to $T = 393$ K these are the mechanisms that are responsible for charge transport in the SBN60 film, and at $T \geq 393$ K, the main contribution begins to be made by Schottky emission at the Ag/Pd/SBN60 interface, which explains the difficulties noted above in measuring the $P(E)$ dependences at these temperatures.

Complex $J(E)$ dependences at $E < 4.5$ MV/m indicate the need for their analysis using modern theories of charge transfer in dielectrics (the Nasyrov–Gritsenko model of phonon-assisted tunneling between traps, the Makram–Ebeid and Lannoo model of multiphonon ionization of isolated traps), which requires detailed studies in this range of electric fields and at lower temperatures.

Figure 5 shows the results of studies of the dielectric characteristics of the sample in a temperature range of $T = 100-500$ K. It can be seen that in the SBN60 film, a typical for FE-relaxors change in $\varepsilon'(T, f)$ and $\varepsilon''(T, f)$ is observed: with increasing temperature in the region of the FE → PE diffuse phase transition maxima are formed on the dependences at $T = T_m$, which shift to the region of high temperatures as the frequency increases. We have failed to describe the T_m dependence on f in the analyzed frequency range by the Arrhenius law, but only using the Vogel–Fulcher relationship (Figure 5, *d*):

$$f = f_0 \exp\left(E_{act}/(k(T_m - T_f))\right), \qquad (2)$$

where f_0 is frequency of attempts to overcome the potential barrier E_{act}, k is Boltzmann constant, T_f is Vogel–Fulcher temperature, interpreted as the temperature of „static freezing“ of electric dipoles.

The calculated values of E_{act}, f_0 and T_f in the SBN60 film were 0.019 eV, $2\cdot10^8$ Hz, and 367 K, respectively. For pure SBN61 single crystals, according

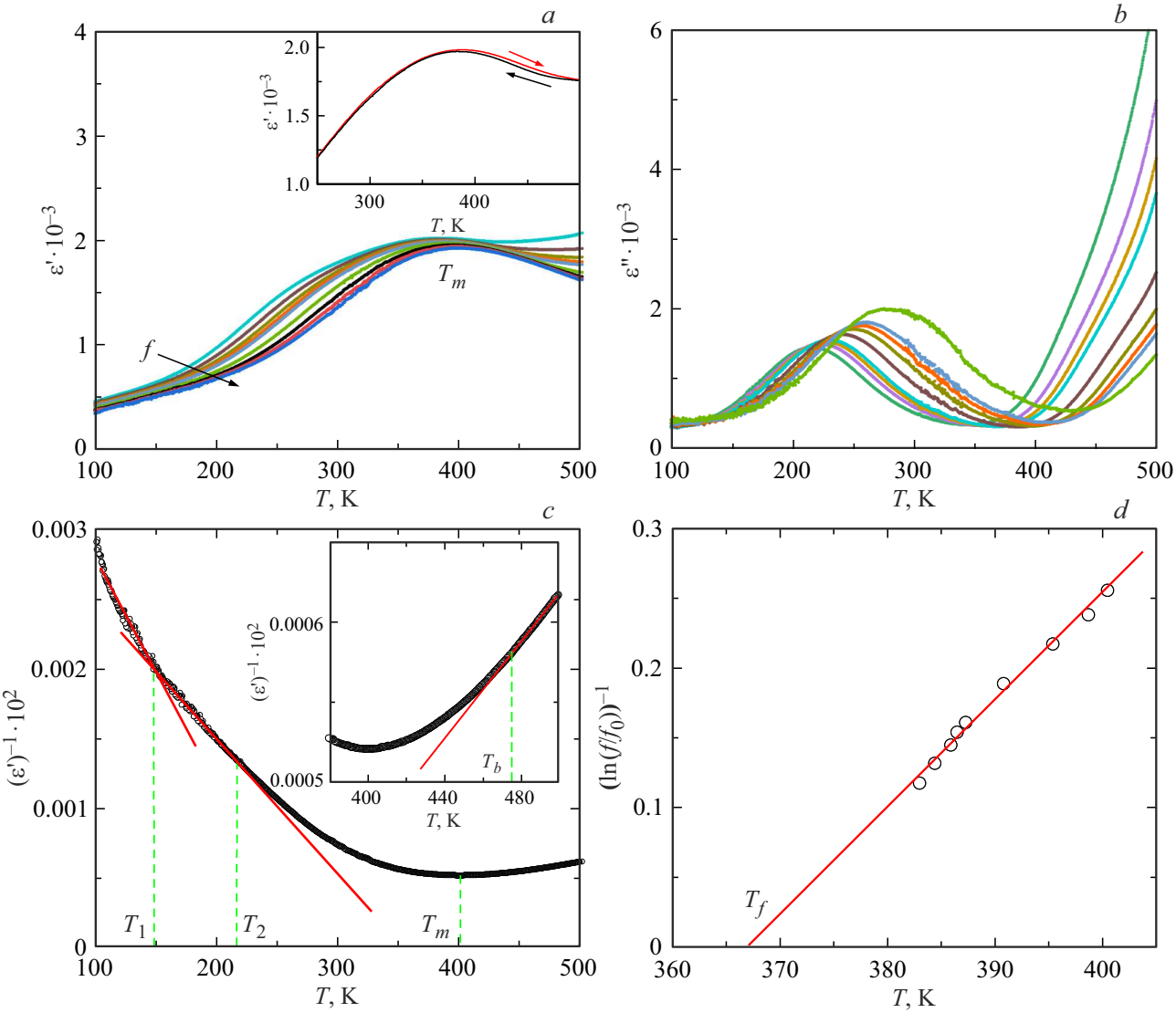

Figure 5. $\varepsilon'(T)$ (a) and $\varepsilon''(T)$ (b) dependences for the SBN60 film at $T = 100-500$ K and $f = 500-10^5$ Hz. c — $(\varepsilon')(T)$ dependence at $f = 10^5$ Hz for the SBN60 film, illustrating the fulfillment of the Curie-Weiss law. d — $\left(\ln(f)-\ln(f_0)\right)^{-1}(T)$ dependence for the SBN60 film, where the straight line is the result of calculation using the Vogel–Fulcher relationship.

to [16] $E_{\text{act}} = 0.023$ eV, $f_0 = 14 \cdot 10^8$ Hz, and $T_f = 330$ K, and for ceramics $E_{\text{act}} = 0.009$ eV, $f_0 = 2.4 \cdot 10^8$ Hz, and $T_f = 326$ K [17]. This indicates that the main mechanism responsible for the dielectric response in the region of FE → PE diffuse PT of the studied barium-strontium niobate, both in the form of thin films and in the form of ceramics and single crystals, is associated with the dynamics of polar nanoregions [16]. As can be seen from Figure 5, c the Burns temperature, T_b, (the temperature below which polar regions appear in ferroelectric relaxors) in the SBN60 film is 475 K and exceeds by ~ 115 K the values of T_b for the SBN61 single crystal [16] and exceeds by ~ 100 K the values for the SBN60 ceramics [17]. The relaxor properties in SBNx solid solution are associated with the disordered arrangement of Sr and Ba atoms in structural positions A1 (channels with a quadrangular cross-section) and A2 (channels with a pentagonal cross-section) [6,16–19], which leads to fluctuations in the chemical composition over the volume of the material, their concentration gradient, as well as a local decrease in symmetry and an internal electric field, which is most likely responsible for the asymmetry of the $P(E)$ dependences in low fields. As shown in [20], in SBN61 single crystals, this leads to the emergence of various metastable and stable states with their lifetimes distributed over a very wide range of values. As a result, the $P(E)$ loops of single crystals become anomalous and hysteresis effects are observed on the $\varepsilon'(T)$ curves. In the films we studied, a small hysteresis of $\varepsilon'(T)$ and $\varepsilon''(T)$ is observed only in the vicinity of T_m (see inset in Figure 5, a). In the low-temperature region ($T < 300$ K) two linear sections were recorded on the $1/\varepsilon'(T)$ dependences — at $80\,\text{K} < T < T_1$ and $T_1 < T < T_2$ (Figure 5, c). Whereas the

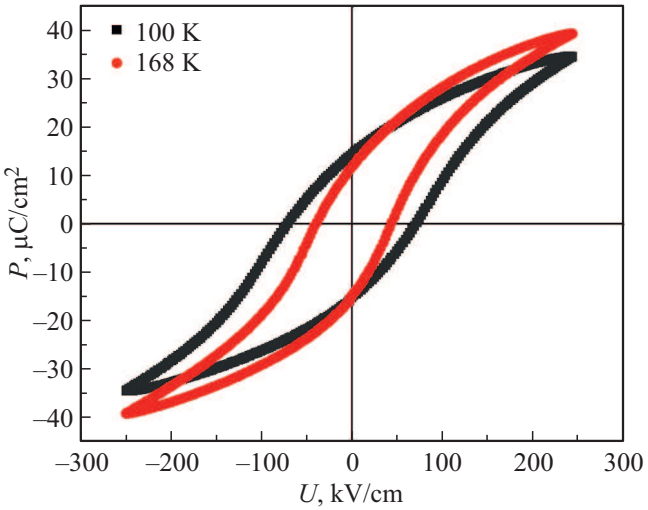

Figure 6. $P(E)$ dependences for the SBN60 film at temperatures of 100 and 168 K.

nature of the occurrence of the anomaly at $T = T_2$ is due to the macroscopic phase transition of the sample to the ferroelectric state, at $T = T_1$, as in the case of SBN61 single crystals [16], it is disputable. Based only on the dielectric studies of films at these temperatures, it is difficult to judge the type of phase transformation at $T = T_1$; the presence of a sharp break of $1/\varepsilon'(T)$ is indicative of a small temperature blurring of the transition, but taking into account the data presented in Figure 6, the phase transformation at these temperatures can be said to occur between two FE phases.

4. Conclusion

Thus, according to X-ray diffraction analysis of the SBN60/Pt/MgO(001) heterostructure, it was established that the grown SBN60 film was undoped and single-crystalline. It is shown that the Poole–Frenkel emission and SCLC are the predominant electrical conductivity mechanisms making the main contribution to the leakage current of the SBN60 film at $T = 303-453$ K and $U = -25-25$ V. A significant increase in leakage currents with increasing temperature is presumably explained by the Schottky emission (due to an increase in the thermionic current).

Studies of the dielectric properties of SBN60 films have shown that, as in the case of single crystals and ceramic samples, barium strontium niobate SBN60 in the form of nanoscale single crystal films is a ferroelectric relaxor. This indicates that fluctuations in the chemical composition over volume inherent in these materials with the structure of unfilled TTB also occur in film structures, and the dielectric response during the FE → PE PT is largely due to the dynamics of polar nanoregions.

It should be noted that taking into account the results of our studies [21,22], we can conclude that in the system of SBN solid solution the compounds with $x \geq 0.5$ both in the form of polycrystalline and single-crystalline films are FE-relaxors. These results are to be included in the synthesis, research, and development of functional elements based on nanoscale SBN films.

Funding

The study was supported by the Ministry of Science and Higher Education of the Russian Federation (State assignment in the field of scientific activity for 2023). Project No. FENW-2023-0010/(GZ0110/23-11-IF).

Conflict of interest

The authors declare that they have no conflict of interest.

References

[1] K.M. Rabe, C.H. Ahn, J-M. Triscone. Fizika segnetoelektrikov: sovremennyi vzglyad, Laboratoriya znanij, M., (2011), 440 s. (in Russian).
[2] V.A. Gritsenko, D.R. Islamov. Fizika dielektricheskikh plenok: mekhanizmy transporta zaryada i fizicheskie osnovy priborov pamyati, Parallel, Novosibirsk, (2017), 352 s. (in Russian).
[3] K.A. Vorotilov, V.M. Mukhortov, A.S. Sigov, Integrirovannye segnetoelektricheskie ustroystva, Energoatomizdat, M., (2011), 175 s. (in Russian).
[4] S. Gupta, S. Sharma, T. Ahmad, A.S. Kaushik, P.K. Jha, V. Gupta, M. Tomar. Mater. Chem. Phys. **262**, 124300 (2021).
[5] S. Ivanov, E.G. Kostsov. IEEE Sensors J. **20**, *16*, 9011 (2020).
[6] Yu.S. Kuzminov. Segnetoelektricheskie kristally dlya upravleniya lazernym izlucheniem Nauka, M., (1982), 400 s. (in Russian).
[7] V. Gopal. J. Appl. Phys. **116**, *8*, 084502 (2014).
[8] G. Velarde, S. Pandya, J. Karthik, D. Pesquera, L.W. Martin. APL Materials **9**, *1*, 010702 (2021).
[9] C. Zhang, Z. Zeng, Z. Zhu, M. Karami, X. Chen. Phys. Rev. Appl. **14**, *6*, 064079 (2020).
[10] S. Lee, R.H. Wilke, S. Trolier-McKinstry, S. Zhang, C.A. Randall. Appl. Phys. Lett. **96**, *3*, 031910 (2010).
[11] H.F. Hung, C.F. Yang, C.C. Wu. Sensors Mater. **29**, *4*, 397 (2017).
[12] A.V. Pavlenko, S.P. Zinchenko, D.V. Stryukov, A.P. Kovtun. Nanorazmernye plenki niobata bariya-strontsiya: osobennosti polucheniya v plazme vysokochasotnogo razryada, struktura i fizicheskie svoistva, YuNTs RAN, Rostov na D., (2022), 244 s. (in Russian).
[13] A.V. Pavlenko, D.V. Stryukov, L.I. Ivleva, A.P. Kovtun, K.M. Zhidel', P.A. Lykov. FTT **63**, *2*, 250 (2021). (in Russian).
[14] F.-C. Chiu. Adv. Mater. Sci. Eng. **2014**, 1 (2014).
[15] S. Zi. Fizika poluprovodnikovykh priborov, Mir, M., (1984), T. 1, 456 s. (in Russian).
[16] E. Buixaderas, M. Savinov, M. Kempa, S. Veljko, S. Kamba, J. Petzelt, R. Pankrath, S. Kapphan. J. Phys.: Condens. Matter. **17**, *4*, 653 (2005).
[17] Y. Zhao, J. Wang, L. Zhang, X. Shi, S. Lui, D. Zhang. Ceram. Int. **42**, *15*, 16697 (2016). doi.org/10.1016/j.ceramint.2016.07.120
[18] V. Krayzman, A. Bosak, H.Y. Playford, B. Ravel, I. Levin. Chem. Mater. **34**, *22*, 9989 (2022).

[19] L. Hongbo, D. Brahim. J. Alloys Comp. **929**, 167314 (2022).
[20] V.V. Gladkiy, V.A. Kirikov, S.V. Nekhlyudov, T.R. Volk, L.I. Ivleva. Pisma v ZhETF **71**, *1*, 38 (2000). (in Russian).
[21] A.V. Pavlenko, D.A. Kiselev, Ya.Yu. Matyash. FTT **63**, *6*, 776 (2021). (in Russian).
[22] A.V. Pavlenko, A.P. Kovtun, S.P. Zinchenko, D.V. Stryukov. Pisma v ZhTF **44**, *11*, 30 (2018). (in Russian).

Translated by Y.Alekseev